big data and cognitive computing

MDPI

Article

Effective Flow Ratio: A Novel Efficiency Metric for Heterogeneous Traffic in a Signalized Urban Intersection with Aerial Computer Vision

Abu Anas Ibn Samad [1], Tanvir Ahmed [1] and Md Nazmul Huda [2,*]

[1] SIGMIND, Dhaka 1215, Bangladesh; abushuvom@sigmind.ai (A.A.I.S.); tanvir.ahmed@sigmind.ai (T.A.)
[2] Department of Electronic and Electrical Engineering, Brunel University of London, Kingston Ln, Uxbridge UB8 3PH, UK
* Correspondence: mdnazmul.huda@brunel.ac.uk

Abstract

Intelligent Transportation Systems (ITS) primarily rely on flow rate and occupancy to estimate traffic states. However, in heterogeneous traffic conditions characterized by weak lane discipline and diverse vehicle classes, these conventional metrics fail to capture the true operational efficiency of signalized intersections. High flow rates can mask underlying inefficiencies, while low flow rates do not necessarily indicate free-flow conditions. This paper introduces a novel computer vision-based metric, the Effective Flow Ratio (EFR), designed to quantify the actual discharge efficiency of mixed traffic. By leveraging Bird's-Eye View (BEV) vehicle tracking using You Only Look Once version 11 (YOLOv11) and ByteTrack, EFR distinguishes between kinematic movement and effective discharge, resolving the ambiguity of "moving but not clearing" states. We analyze 21 days of continuous footage from a rooftop-mounted camera overlooking a congested intersection in Dhaka, Bangladesh, exhibiting distinct non-linear behaviors compared to raw flow counts. Our results demonstrate that: (i) Flow rate and discharge efficiency are dynamically decoupled, evidenced by significant variance in EFR within identical flow bins; (ii) Temporal rolling correlations reveal transient regimes where traditional signal control logic would misinterpret congestion severity; and (iii) EFR provides a more robust proxy for intersection performance than occupancy or volume alone. The proposed metric offers a granular, physics-informed input for next-generation adaptive traffic signal control in developing urban environments.

Keywords: heterogeneous traffic; Effective Flow Ratio; computer vision; intelligent transportation systems; signal control; traffic state estimation

Academic Editor: Carson K. Leung

Received: 12 January 2026
Revised: 2 March 2026
Accepted: 2 March 2026
Published: 6 March 2026

1. Introduction

The operational dynamics of signalized intersections in the rapidly densifying urban centers of the Global South—exemplified by cities such as Dhaka, Delhi, and Jakarta—diverge fundamentally from the idealized traffic stream models that underpin classical transportation engineering. In these environments, traffic is not a uniform flow of automobiles confined to discrete lanes but a heterogeneous, granular suspension of diverse agents: private cars, buses, motorcycles, cycle rickshaws, and pedestrians [1–3]. These agents interact with limited lane discipline, creating a stochastic friction that defies the deterministic assumptions of standard performance metrics such as Level of Service (LOS), Degree of Saturation (DoS), and Average Delay [4–7].

The evolution of Intelligent Transportation Systems has spurred diverse research directions, ranging from mathematical modeling of cyber-attack resilience in connected environments [8,9], to the empirical development of vision-based efficiency metrics for heterogeneous traffic. However, in practice, traditional traffic management systems rely heavily on the correlation between signal allocation (supply) and flow counts (demand). The implicit assumption governing these systems is that the provision of green time to a queued approach will automatically result in vehicular discharge at a predictable saturation flow rate. However, in mixed-traffic environments characterized by frequent lateral interference, downstream spillback, and non-motorized vehicle (NMT) encroachments, this assumption breaks down [10–13]. Vehicles may be physically present within the detection zone, and the signal may be green, yet effective movement is arrested by localized conflicts. Under such conditions, inductive loop detectors or simple line-crossing counters may register high "presence" or even moderate "flow" (as vehicles creep past a point), masking the underlying reality that the intersection's discharge efficiency has collapsed [14,15].

This decoupling of flow rate from operational efficiency creates a critical measurement gap. When high flow counts coexist with high latency, traditional metrics fail to diagnose the root cause, often leading to the misallocation of green time in adaptive signal control strategies. To bridge this gap, traffic monitoring must evolve from simple Eulerian counting (measuring flux at a boundary) to Lagrangian state estimation (measuring the motion dynamics of agents within the control volume). Eulerian metrics, such as flow rate, are fundamentally limited because they aggregate vehicle crossings without distinguishing between efficient discharge and slow creeping motion. In contrast, Lagrangian tracking follows individual vehicle trajectories, enabling direct observation of kinematic states and velocity profiles [16–18].

This paper introduces a novel, computer-vision-driven framework to operationalize this shift. We propose Flow Ratio—the proportion of vehicles exhibiting kinetic motion among all present—as a first-order state variable. We further refine this into the Effective Flow Ratio (EFR), a second-order metric that weights kinetic motion by discharge quality, penalizing the slow, creeping flow characteristic of congested mixed traffic. By leveraging high-resolution aerial Bird's-Eye View (BEV) imagery processed via YOLOv11 detection [19] and ByteTrack multi-object tracking [20], we extract these metrics in real-time, resolving the "moving but not clearing" ambiguity that plagues current sensor networks.

The primary contribution of this study is not a new signal control algorithm, but the definition and validation of the state variables necessary to enable such control in heterogeneous environments. Using a comprehensive dataset from a major intersection in Dhaka, Bangladesh, we empirically demonstrate that Flow Rate and EFR are dynamically decoupled, revealing latent inefficiencies invisible to classical analysis. This work provides the foundational metrics required to transition Intelligent Transportation Systems (ITS) from volume-based logic to efficiency-based logic in the complex traffic landscapes of the developing world.

The specific objectives of this study are:

- To define and operationalise Flow Ratio as a BEV computer-vision-derived metric reflecting kinematic movement presence in mixed traffic.
- To introduce Effective Flow Ratio (EFR) as an operational efficiency metric that weights movement by discharge quality through a velocity efficiency index, capturing the "moving but not clearing" phenomenon.
- To empirically demonstrate the temporal decoupling between flow rate and EFR at a signalized Dhaka intersection through rolling correlation and flow-binned distribution analyses.

- To validate that EFR reveals operational inefficiencies invisible to traditional signal-flow perspectives, motivating its integration into monitoring and adaptive control strategies.

2. Related Work

2.1. Limitations of Classical Performance Metrics in Heterogeneous Traffic

Urban intersections in developing countries operate under fundamentally different conditions than those in developed nations. In cities such as Dhaka, Delhi, Jakarta, and other South Asian urban centers, traffic streams comprise a diverse mixture of vehicles including cars, buses, motorcycles, auto-rickshaws, cycle-rickshaws, and pedestrians, all operating with minimal lane discipline [1–3]. This heterogeneous, non-lane-based traffic environment creates operational characteristics that diverge significantly from the idealized, orderly traffic streams assumed in classical traffic engineering models [4,5].

Traditional performance metrics—including Level of Service (LOS), degree of saturation (DoS), and average delay—were originally formulated for homogeneous traffic streams where vehicles are assumed to operate in distinct lanes with predictable following and crossing behavior. The Highway Capacity Manual (HCM), the primary U.S. reference for capacity and LOS analysis, explicitly recommends procedures based on steady-state assumptions and uniform vehicle behavior patterns [21]. However, these metrics often fail to capture the actual movement efficiency in heterogeneous traffic due to several critical disconnects:

- **LOS Inadequacy:** LOS classification relies on speed and density thresholds calibrated exclusively for homogeneous traffic. Research from South and Southeast Asia demonstrates that applying HCM methodology directly to heterogeneous conditions produces unreliable results, with capacity estimates deviating significantly (>50%) from observed field values [11,22–24].
- **Degree of Saturation Opacity:** DoS, calculated as demand/capacity, provides no information about whether vehicles physically present in an intersection approach are actually moving. Vehicles may be stationary due to pedestrian interference, lane blockages, or spillback, yet are still counted in volume-based flow measurements [1,10–13].
- **Signal-Flow Decoupling:** The fundamental assumption that green time and available capacity automatically translate into throughput breaks down under heterogeneous conditions. Strong correlation between signal allocation and flow volume may coexist with poor movement efficiency due to pedestrian interference, non-motorized vehicle encroachments, or spillback from downstream intersections [1,7].
- **Free Flow Condition Uncertainty:** Identifying free-flow conditions in heterogeneous traffic is complicated by the presence of diverse vehicle types operating at different desired speeds. Research on Indian highways showed that conventional headway-based approaches (3.0 s per HCM) are inadequate; heterogeneous traffic requires gap thresholds of 2.6–3.5 s depending on vehicle composition and driver behavior [25,26]. Similarly, trajectory-based analysis of lane-changing behavior [27] demonstrates the necessity of granular motion data to understand complex driver interactions, a requirement that becomes even more critical in heterogeneous environments where lateral friction is dominant.
- **Saturation Flow Rate Variability:** Saturation flow rate exhibits considerable variability based on traffic composition, degree of saturation, and vehicle maneuverability. Recent Bayesian MCMC research applying rigorous statistical methods to heterogeneous traffic in Indonesia demonstrated that conventional linear capacity models significantly overestimate saturation flow, with errors exceeding 50% [22].

2.2. Pedestrian Interference and Non-Motorized Vehicle Effects on Intersection Performance

Pedestrian behavior at signalized intersections significantly affects vehicular discharge efficiency, particularly in urban areas with high crossing demand. Classic studies on pedestrian–vehicle conflicts demonstrate that exclusive pedestrian phasing (EPP), while theoretically improving safety by eliminating crossing conflicts, can paradoxically increase overall intersection delay and encourage non-compliant pedestrian crossing behavior due to extended waiting times [28,29]. In contrast, concurrent pedestrian phasing (CPP), though involving some pedestrian–vehicle conflicts, may produce better overall operational efficiency and higher pedestrian compliance, highlighting the inherent trade-offs between safety and mobility.

The presence of non-motorized vehicles (NMVs) including cycle-rickshaws, hand-drawn rickshaws, and motorized three-wheelers represents a unique challenge in South Asian traffic systems. These vehicles are characterized by irregular lane positioning, slow speeds, frequent stops for passenger pickup and drop-off, and unpredictable lateral movements [3,29]. Research on the impact of three-wheelers on traffic flow in India utilizing artificial neural network approaches demonstrates that vehicles of all types experience speed reductions of 4–35% in the presence of significant three-wheeler populations, with cascading effects on intersection capacity [30].

2.3. Computer Vision-Based Detection and Tracking Technologies

2.3.1. YOLO Detection Model Evolution

Recent advances in deep learning have revolutionized traffic monitoring through automated video analysis. The YOLO (You Only Look Once) family of real-time detectors has evolved significantly, with each successive version achieving incremental improvements in detection accuracy, inference speed, and handling of edge cases. Comparative studies [19,31,32] have demonstrated that YOLOv11 achieves superior mean average precision (mAP@0.5 = 0.773) compared to predecessors like YOLOv8 (0.632) and YOLOv10 (0.714), particularly in detecting small and clustered objects typical of heterogeneous traffic. While maintaining real-time inference speeds (7.8 ms), YOLOv11's architectural improvements, such as the C2PSA block, provide the necessary robustness for identifying diverse vehicle classes including rickshaws and bicycles in dense urban scenes. Crucially, this architectural resilience directly addresses the environmental constraints highlighted by recent literature; the model's superior feature extraction capabilities provide the necessary margin to maintain identity persistence even under the adverse conditions typical of the Global South, such as low-light environments and heavy monsoon rains, which frequently exacerbate the creeping behavior of congested traffic. Furthermore, to address the inherent challenge of detecting small objects such as motorcycles and bicycles that appear at minimal pixel resolutions from aerial perspectives, Slicing Aided Hyper Inference (SAHI) [33] can be integrated with YOLO-based detectors to significantly improve detection accuracy across diverse scenarios by processing image slices at higher effective resolutions.

2.3.2. Multi-Object Tracking Algorithm Comparison and Selection Rationale

Multi-object tracking (MOT), essential for maintaining vehicle identity continuity across video frames, has been advanced by several algorithms including SORT (Simple Online and Realtime Tracking), DeepSORT, and ByteTrack. A comprehensive comparative evaluation [34] demonstrates significant performance differences in Table 1.

The ByteTrack algorithm (Selected for this study) achieves state-of-the-art MOTA (77.3%) via cascaded association strategy, maintaining low ID switches (558) with high processing speed (171 FPS) suitable for real-time applications. We prioritized this high-throughput architecture because it ensures minimal computational overhead (approx.

6 ms inference per frame). This speed is critical for preventing bottlenecks in the data pipeline, ensuring that the system remains viable for real-time traffic signal actuation where low-latency state estimation is a prerequisite for effective control. ByteTrack utilizes both high-confidence and low-confidence detections through two-phase Hungarian algorithm matching, demonstrating superior performance in occlusion-heavy heterogeneous traffic [20].

Table 1. Multi-Object Tracking Algorithm Performance Comparison (Adapted from [34]).

Metric	SORT	DeepSORT	ByteTrack
MOTA (%)	54.7	61.4	77.3
MOTP (%)	77.5	79.1	82.6
ID Switches (count)	831	781	558
Mostly Tracked (%)	34.2	45.1	54.7
Mostly Lost (%)	24.6	21.3	14.9
False Positives (count)	7876	5604	3828
False Negatives (count)	26,452	21,796	14,661
Processing Speed (FPS)	143	61	171

2.4. Aerial Bird's-Eye View Monitoring for Traffic Analysis

Unmanned aerial vehicles (UAVs) equipped with mounted cameras provide unique advantages for traffic surveillance by capturing aerial Bird's-Eye View (BEV) imagery that eliminates perspective distortion and reduces occlusions inherent in ground-level fixed-camera views [32,35]. The VisDrone dataset, a large-scale benchmark for training and evaluating aerial detection models, has become the standard for training and evaluating aerial detection models, with specific focus on handling the unique challenges of aerial imagery including scale variation, small object detection, and clustered instances [20,35].

2.5. Comparison of Traffic Performance Metrics and Identification of Conceptual Gap

Table 2 shows that classical metrics (flow rate, degree of saturation, LOS, delay, queue length) describe demand, capacity, or time allocation but never verify whether vehicles present in the approach are actually moving. In heterogeneous traffic, this makes them blind to conditions where green time and high demand coexist with largely stationary queues. Flow Ratio closes this gap by using BEV video and motion classification to measure the share of moving vehicles among all present, directly quantifying movement efficiency instead of relying on indirect proxies.

Table 2. Comparison of Traffic Performance Metrics and Identification of Conceptual Gap. Standard definitions are derived from the Highway Capacity Manual [21], while limitations in heterogeneous traffic are synthesized from recent studies [1,10–13].

Metric	Definition	Data Source	Applicability to Heterogeneous Traffic	Key Limitation
Flow Rate (vehicles/min)	Volume of vehicles crossing a line per unit time	Line-based counting (manual, video, detector)	Moderate— captures demand but not movement quality	Conflates moving and stationary vehicles
Degree of Saturation (v/c)	Ratio of demand to capacity	Detector counts + signal timing	Low—assumes homogeneous vehicle interactions	No information on whether vehicles are actually moving
Level of Service (LOS)	Qualitative grade A–F based on speed/density	Speed surveys + capacity analysis	Low—thresholds calibrated for homogeneous traffic	Produces unreliable classifications in heterogeneous conditions
Average Delay	Difference between actual and ideal travel time	Queue observation or trajectory data	Moderate—valid metric but difficult to measure	Requires queue length estimation with inherent uncertainties

Table 2. *Cont.*

Metric	Definition	Data Source	Applicability to Heterogeneous Traffic	Key Limitation
Queue Length	Physical extent of vehicle queue	Detector placement + estimation models	Low—estimation fails in heterogeneous traffic with occlusions	Detector-based methods unreliable; visual measurement difficult
Signal Timing Efficiency	Ratio of effective green time to cycle length	Signal timing data	Low—does not account for green-to-discharge conversion	Assumes that allocated green time equals vehicle movement
Effective Flow Ratio (EFR) (proposed)	Velocity-weighted proportion of moving vehicles, representing actual discharge quality	Aerial BEV video + trajectory tracking	High—directly measures operational efficiency and penalizes creeping flow	Depends on tracking continuity and accurate crossing time measurement

2.6. Summary and Research Gap

While existing literature provides robust metrics for homogeneous lane-based traffic such as saturation flow, delay estimation, Level of Service (LOS), and Degree of Saturation (DoS), these methods consistently fail to capture the stochastic dynamics of heterogeneous traffic prevalent in the Global South. Simultaneously, the field of computer vision has advanced significantly by transitioning from simple presence detection to complex trajectory analysis. Our own previous research has contributed to these foundational capabilities by establishing frameworks for occlusion resilient vehicle counting via a Multi-Line Aggregated Tracking (MLAT) approach [36] and detailed fine-grained multi-class vehicle classification tailored for heterogeneous environments using the MVINet deep learning architecture [37]. However, despite these advancements in counting and classifying vehicles, a critical research gap remains regarding the lack of operational metrics that quantify the efficiency of discharge. Accurate enumeration alone cannot distinguish between a vehicle that is flowing freely and one that is creeping through a congested intersection. This study bridges that specific gap by moving beyond static counts to formulate the Effective Flow Ratio (EFR), a dynamic efficiency metric derived from aerial vision that reveals the hidden inefficiencies invisible to traditional volume-based methods.

3. Methodology

3.1. Conceptual Framework: From Eulerian Counting to Lagrangian Efficiency

To address the limitations of classical metrics in heterogeneous traffic, we introduce a conceptual hierarchy that bridges the gap between demand measurement and efficiency diagnosis. Traditional traffic engineering relies on the fundamental diagram of traffic flow: $q = k \cdot u$, where q is flow, k is density, and u is speed. In homogeneous traffic, these variables are tightly coupled. However, in heterogeneous traffic, the effective density k becomes unmeasurable due to the lack of lane discipline. A discrete count of vehicles does not translate to density because the "passenger car unit" (PCU) varies dynamically with lateral clearances and composition.

Consequently, the standard metric, Degree of Saturation ($X = v/c$), fails because the capacity (c) is not a static constant but a stochastic variable dependent on instantaneous friction (e.g., a rickshaw blocking multiple effective lanes). Flow rate (v) can remain high even when actual discharge efficiency drops, implying that the denominator (c) has collapsed.

We propose three observables that capture fundamentally different operational dimensions:

- **Flow Rate** (F_d): Demand throughput (vehicles per time)—an Eulerian boundary measurement
- **Flow Ratio** (R_d): Movement presence (fraction of vehicles moving)—a first-order Lagrangian kinematic metric

- **Effective Flow Ratio** (EFR): Discharge quality (velocity-weighted movement)—a second-order Lagrangian operational metric

EFR subsumes Flow Ratio while preserving interpretability. These three variables should not be interpreted interchangeably: while flow rate indicates demand, only EFR reveals whether that demand is being served efficiently under friction from non-motorized vehicles and pedestrians.

3.2. Theoretical Basis: Limit Analysis of EFR

Before defining the metrics formally, we establish the theoretical soundness of EFR through limit analysis. The proposed Effective Flow Ratio acts as a proxy for the efficiency of capacity utilization. Consider the behavior of EFR at operational extremes:

1. **Free Flow Regime:** All vehicles moving ($S_d = 0$) at free-flow speed ($T_{\text{actual}} \approx T_{\text{ideal}}$). Here, velocity efficiency $E_v \approx 1$ and $M_d \approx N_d$. Thus, EFR ≈ 1, correctly identifying optimal efficiency.
2. **Jam Density:** All vehicles static ($M_d = 0$). Here, EFR $= 0$, correctly identifying complete gridlock.
3. **The "Creeping" State (The Heterogeneous Trap):** All vehicles are moving ($M_d \approx N_d$), but slowly ($T_{\text{actual}} \gg T_{\text{ideal}}$).
   - Classical Flow Ratio: $R_d \approx 1$ (suggesting high efficiency)
   - Effective Flow Ratio: EFR $\approx T_{\text{ideal}}/T_{\text{actual}} \ll 1$ (correctly identifying inefficiency)

This limit analysis confirms that EFR is the superior metric for the specific problem of "moving but not clearing" identified in the abstract. The creeping state is precisely where Flow Ratio fails and EFR succeeds—when vehicles exhibit motion but fail to discharge efficiently due to heterogeneous friction.

3.3. The Illusion of Efficiency in Signal-Flow Correlation

While signal status (G_d) and flow rate (F_d) often correlate strongly in classical analyses, this relationship can be deceptive under heterogeneous conditions. To illustrate this "false positive" efficiency, Figure 1 presents a temporal overlay of signal status versus flow rate.

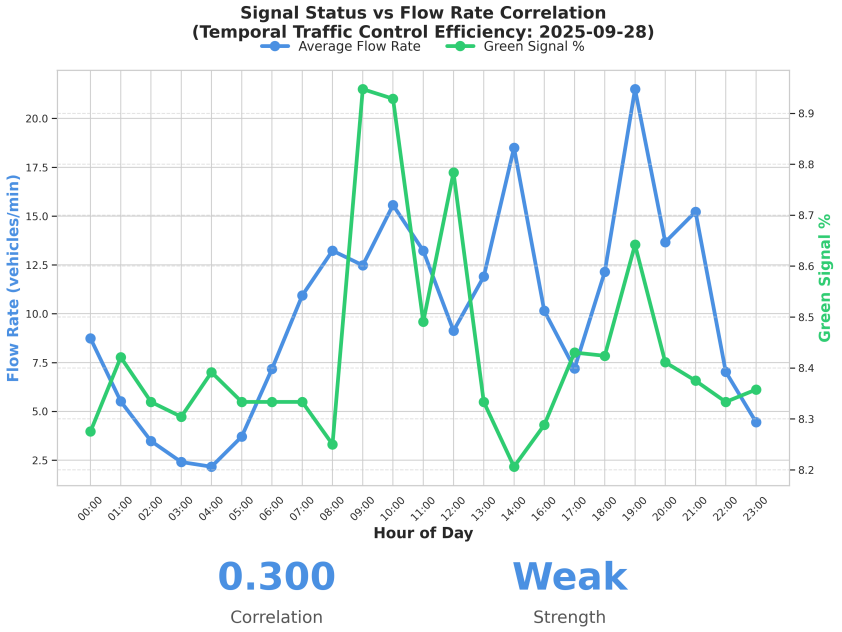

Figure 1. The Illusion of Efficiency. Signal-flow correlation may appear strong even when actual movement efficiency is poor. The divergence between signal allocation (green) and true discharge quality highlights that high flow rate does not guarantee effective movement in mixed traffic.

The visualization exposes a critical operational failure. At specific peak intervals (e.g., 09:00 and 19:00), the green signal allocation (green line) tracks closely with the average flow rate (blue line), suggesting a responsive system. In a standard report, this alignment would imply optimal performance. However, ground truth observation reveals that despite this apparent synchronization, movement efficiency was often poor due to pedestrian interference and rickshaw blockage. This creates an Illusion of Efficiency where the infrastructure supplies green time and sensors record volume, but the actual discharge quality is low. By incorporating Flow Ratio, the analysis reveals whether demand volume actually converts into vehicle motion. This motivating example justifies the development of Flow Ratio and EFR as necessary ground-truth variables.

3.4. Data Acquisition and Processing Pipeline

To operationalize the EFR metric, we employ a multi-source sensing framework that captures both flow demand and motion efficiency. The methodological pipeline, illustrated in Figure 2, integrates three parallel data streams into a central fusion block:

1. **Aerial View System (Lagrangian):** This module processes the aerial video through Multi-Object Tracking to perform Motion Analysis. By applying velocity thresholds to separate "Moving" from "Static" vehicles, it directly computes the Flow Ratio ($R_d(t)$) as the proportion of moving agents.
2. **Ground View System (Eulerian):** Simultaneously, line-based counting is used to calculate the standard Flow Rate ($F_d(t)$) and perform approach assignment, establishing the baseline demand volume.
3. **Signal Controller System:** The system interfaces with the controller API to log Phase States ($g_{t,d}$) and calculate exact Green Seconds ($G_{c,d}$) per cycle.

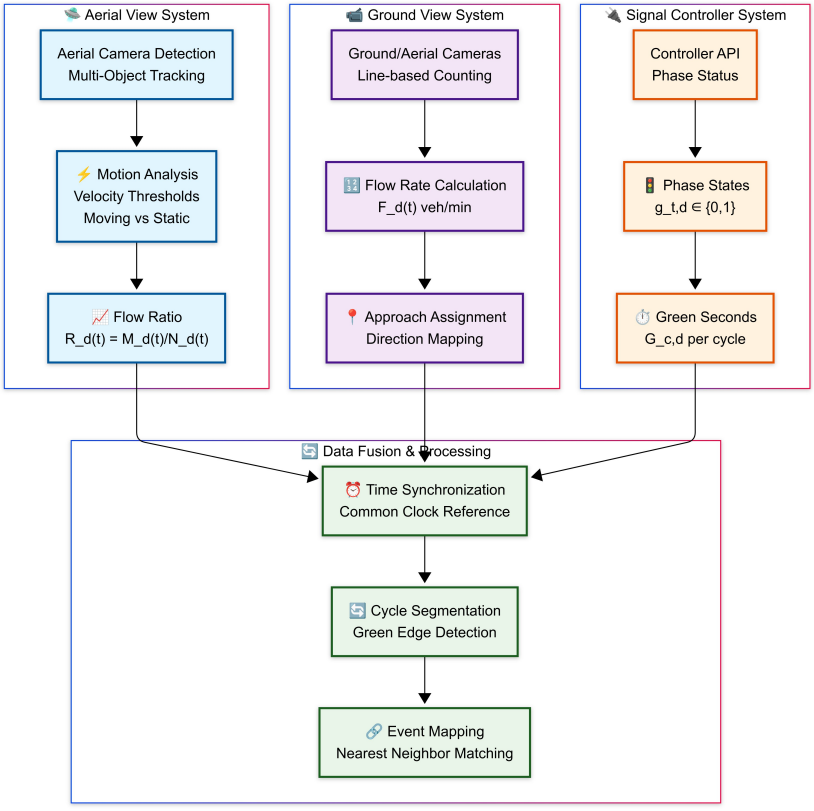

Figure 2. The methodological pipeline for EFR computation. The framework fuses three independent systems—Aerial (tracking), Ground (counting), and Signal (timing)—through a central Data Fusion and Processing block to derive synchronized efficiency metrics.

The physical configuration of the sensing environment is shown in Figure 3. To overcome the severe occlusion challenges typical of mixed traffic, where buses frequently block the view of smaller rickshaws and motorcycles, we employed a fixed rooftop-mounted camera installed on an adjacent 18-story building at approximately 55 m altitude. This permanent installation provides an orthogonal Bird's-Eye View (BEV) of the entire intersection without the regulatory, durability, and flight-time constraints of drone-based platforms. This perspective is critical for the Aerial View System because it allows the computer vision model to track vehicles deep within the queue, rather than just those at the stop line. As seen in the figure, this setup captures the complex, non-lane-based interactions across all four approaches simultaneously, serving as the ground truth for calibrating intersection-wide analytics.

Figure 3. Data acquisition setup. The 4K rooftop camera provides an occlusion-free Bird's-Eye-View (BEV) at 55 m altitude. This fixed infrastructure enables continuous, uninterrupted data collection while capturing the tracking of deep queues and lateral interactions that ground-level sensors miss due to occlusion.

3.5. Flow Ratio Definition

For each approach d at time t, let $M_d(t)$ denote the number of moving vehicles and $N_d(t)$ the total number of vehicles (moving + static) within the region of interest (ROI). We define:

$$R_d(t) = \frac{M_d(t)}{N_d(t) + \varepsilon}, \tag{1}$$

where $\varepsilon = 10^{-6}$ prevents division by zero, with results confirmed to be numerically insensitive to this choice. $R_d(t) \in [0, 1]$ reflects the fraction of vehicles exhibiting motion presence within the approach. However, motion presence alone does not guarantee effective discharge—a vehicle may be moving slowly or stalled in local conflict without crossing the intersection.

3.6. Effective Flow Ratio (EFR)

To address the limitation that Flow Ratio captures only kinematic presence (Is the vehicle moving at all?) rather than operational efficiency ("Is the vehicle effectively discharging"), we introduce the Effective Flow Ratio (EFR). This metric weights motion by discharge quality through a Velocity Efficiency Index.

3.6.1. Velocity Efficiency Index

Let $T_{\text{actual},d}(t)$ denote the harmonic mean crossing time for vehicles in approach d during interval t, measured from entry to exit of the intersection ROI. The harmonic mean

is used because it better represents the time required for collective discharge, giving higher weight to slower vehicles that bottleneck the stream. We define the Velocity Efficiency Index as:

$$E_{v,d}(t) = \min\left(1, \frac{T_{\text{ideal}}}{T_{\text{actual},d}(t)}\right), \tag{2}$$

where $T_{\text{ideal}} = 20$ s is a geometry-dependent parameter, not an arbitrary threshold. This value represents the theoretical free-flow traversal time derived from the intersection geometry: with an ROI length of approximately $L \approx 60$ m and a conservative free-flow speed of $v_{\text{free}} \approx 3$ m/s (accounting for the natural slowness of mixed traffic including rickshaws even in uncongested states), we obtain $T_{\text{ideal}} = L/v_{\text{free}} \approx 20$ s. This geometry-based derivation ensures reproducibility across different intersection sizes by scaling T_{ideal} according to local dimensions. It is important to note that T_{ideal} serves as a stream-level baseline for intersection discharge diagnosis rather than a per-class optimal benchmark. Developing class-conditioned baselines remains a subject for future work. When actual crossing time equals or exceeds the ideal, $E_v \leq 1$; longer crossing times (indicating slow discharge due to friction) reduce efficiency proportionally.

3.6.2. EFR Formulation

The Effective Flow Ratio combines motion presence with discharge quality:

$$\text{EFR}_d(t) = \frac{M_d(t) \cdot E_{v,d}(t)}{M_d(t) + S_d(t) + \varepsilon}, \tag{3}$$

where $S_d(t)$ denotes the number of static vehicles in approach d. Since $N_d(t) = M_d(t) + S_d(t)$, EFR can be equivalently expressed as the product of Flow Ratio and Velocity Efficiency:

$$\text{EFR}_d(t) = R_d(t) \cdot E_{v,d}(t). \tag{4}$$

This formulation clarifies the interpretability of EFR: a value of EFR $= 0.5$ may arise from either 50% motion presence with 100% velocity efficiency, or 100% motion presence with 50% velocity efficiency. Unlike raw Flow Ratio, EFR penalizes scenarios where vehicles move but discharge slowly due to pedestrian interference, non-motorized vehicle encroachments, or queue spillback. In this formulation:

- **High EFR** indicates vehicles are moving *and* discharging efficiently.
- **Low EFR with high motion count** signals movement without effective discharge—the target inefficiency this paper aims to expose.
- **EFR is not monotonic with flow rate**, as higher demand does not guarantee higher efficiency in heterogeneous traffic.

3.6.3. Parameter Sensitivity Analysis

The velocity threshold $v_{\min} = 0.5$ m/s (≈1.8 km/h) represents the minimum displacement rate to classify a vehicle as "moving." This threshold was selected to distinguish genuine kinematic motion from detection noise and vibration artifacts. Vehicles below this threshold exhibit negligible spatial displacement across consecutive frames and are classified as stationary.

The ideal crossing time $T_{\text{ideal}} = 20$ s is derived from intersection geometry as described above. To assess sensitivity, we evaluated EFR behavior presented in Table 3 under alternative parameterizations.

Table 3. Sensitivity of EFR to T_{ideal} parameterization with quantitative impact.

T_{ideal} (s)	Interpretation	Mean EFR	σ_{EFR}	Regime Proportions (S/M/E) [a]	Rank ρ [b]
15	Aggressive (faster free-flow)	0.31	0.24	42%/38%/20%	0.97
20	Baseline (geometry-derived)	0.38	0.21	35%/40%/25%	1.00
25	Conservative (slower free-flow)	0.44	0.18	28%/42%/30%	0.96

[a] S = Suppressed (EFR < 0.3), M = Moderate (0.3–0.7), E = Efficient (EFR > 0.7). [b] Spearman rank correlation of per-minute EFR values against the baseline ($T_{\text{ideal}} = 20$ s) parameterization.

Across all parameterizations, the qualitative findings—decoupling of flow and efficiency, and regime identification—remain robust. The baseline value of 20 s provides the most balanced discrimination between operational states, while the near-unity rank correlations ($\rho \geq 0.96$) confirm that the relative ordering of efficiency across time intervals is preserved regardless of the specific T_{ideal} value chosen.

3.7. Flow Rate Measurement

Per-minute flow rate $F_d(t)$ is computed as:

$$F_d(t) = \frac{C_d(t)}{\Delta t}, \tag{5}$$

where $C_d(t)$ is the number of vehicles crossing a designated counting line within interval $\Delta t = 60$ s. This conventional measure captures demand but not necessarily efficiency.

3.8. Correlation Analysis

To evaluate how flow translates into movement efficiency, we analyze the correlation between $F_d(t)$ and $R_d(t)$. Using Pearson's correlation:

$$\rho_{FR,d} = \frac{\sum_t (F_d(t) - \bar{F}_d)(R_d(t) - \bar{R}_d)}{\sqrt{\sum_t (F_d(t) - \bar{F}_d)^2 \sum_t (R_d(t) - \bar{R}_d)^2}}, \tag{6}$$

where $\bar{F}_d$ and $\bar{R}_d$ are temporal means.

3.9. Interpretation

- High F_d with low $R_d \Rightarrow$ latent inefficiency (e.g., spillback, pedestrian/NMT interference).
- High F_d with high $R_d \Rightarrow$ smooth discharge, efficient use of green time.
- Low correlation $\rho_{FR,d}$ across cycles $\Rightarrow$ inconsistent performance requiring signal or demand management.

Thus, Flow Ratio not only complements flow rate but also provides an operational lens into how well demand is translated into actual vehicle movement under mixed-traffic conditions. Correlation analysis was performed both for Flow Ratio and EFR; results presented here focus on EFR as the higher-order metric.

3.10. Pipeline Performance and Robustness

The end-to-end computer vision pipeline was deployed on-device and achieved runtime performance of 10–13 frames per second (FPS), sufficient for the minute-level aggregation employed in this study. Pipeline validation metrics are summarized in Table 4.

Table 4. Computer vision pipeline performance metrics.

Metric	Value	Definition
End-to-end processing rate	10–13 FPS	Frames processed per second (detection + tracking + metric computation)
Vehicle detection rate	95.6%	Proportion of vehicles in frame successfully detected (automated count)
Tracking success rate	98%	Proportion of detections maintaining consistent ID across trajectory
Peak simultaneous detections	232 objects (avg)	Maximum concurrent tracked objects in a single frame

3.10.1. Validation Protocol

To establish a traceable manual baseline tailored to our Lagrangian approach, we conducted a sample-based manual validation study. Because exhaustive frame-by-frame pixel annotation is computationally prohibitive for this operational environment, and because the Effective Flow Ratio (EFR) metric fundamentally relies on trajectory continuity rather than momentary Eulerian presence, we focused our manual ground-truthing directly on trajectory ID persistence.

Two independent human annotators reviewed the raw video across 20 representative 5-min segments (100 min total), capturing a cross-section of morning peak, off-peak, and evening peak conditions. Within these segments, annotators manually tracked a random ground-truth sample of 1000 vehicles (50 per segment, explicitly encompassing cars, buses, motorcycles, and rickshaws). Each vehicle in the sample was visually tracked from ROI entry to exit to verify ID persistence and correct kinematic state classification (moving vs. static) with informal spot-checking applied to ensure agreement.

Evaluated against this manual sample ($n = 1000$), the automated pipeline maintained correct, unbroken track IDs for over 95% of the sampled trajectories. This diagnostic validation explicitly defines the sample size, included classes, and annotation procedure, confirming that the automated association statistics reported in Table 4 align closely with human-verified ground truth. Consequently, this manual audit verifies that the pipeline reliably captures the trajectory continuity required for robust EFR estimation.

3.10.2. Occlusion Handling and Track Continuity

ByteTrack maintains trajectory continuity through Kalman filter-based motion prediction, enabling ID persistence during temporary occlusions lasting up to 30 frames ($\approx$ 1 s at 30 FPS input rate). When a vehicle is temporarily occluded (e.g., by a double-decker bus), the tracker predicts its position and re-associates the detection upon reappearance. This mechanism reduces track fragmentation and ID switches that would otherwise inflate the static vehicle count $S_d(t)$ or introduce spurious crossing time measurements.

3.10.3. Systematic Error Considerations

Several systematic errors may affect the computed metrics:

- **Detection failures:** Missed detections (4.4% of vehicles) cause underestimation of $N_d(t)$. However, since both $M_d(t)$ and $S_d(t)$ are affected proportionally, the Flow Ratio $R_d(t)$ remains relatively stable.
- **Track fragmentation:** ID switches may cause a single vehicle to be counted multiple times in crossing time computations. The 98% tracking success rate and ByteTrack's re-identification logic mitigate this effect.
- **Small target detection:** Motorcycles and bicycles at the 55 m altitude appear as small targets ($\sim$20–40 pixels). The YOLOv11 model, pre-trained on the VisDrone aerial

dataset, is specifically optimized for such scenarios, though detection confidence for these classes is lower than for larger vehicles.

These considerations inform the interpretation of results but do not fundamentally alter the observed flow–efficiency decoupling patterns.

3.11. Implementation Details: ROI Construction and Entry/Exit Timing

To ensure full reproducibility, this subsection specifies the computational procedures for ROI definition, entry/exit event detection, and crossing time measurement as implemented in the deployed system.

3.11.1. ROI Geometry and Approach Assignment

Each intersection approach is represented by a configurable polygonal Region of Interest (ROI) defined directly in the 960×960 pixel image domain. Due to the high-altitude (55 m) near-orthogonal perspective, the camera view approximates a Bird's-Eye View (BEV) sufficiently well for flow analysis without requiring a homography transformation to a ground-plane coordinate system. We operate in the image plane to avoid introduction of reprojection errors. To reconcile image-plane operations with metre-based parameters such as v_{free} and $v_{\min}$, a ground-distance reference measurement was used to obtain a metres-per-pixel calibration (yielding approximately 2.54 continuous meters of ground distance equivalent to 1 pixel displacement at the intersection center). ROI vertices for the deployed configuration are provided in the Appendix A. Point-in-polygon membership is determined via ray-casting: for a vehicle centroid (c_x, c_y) and a polygon with n vertices $\{(p_{x_i}, p_{y_i})\}_{i=1}^{n}$, a horizontal ray is cast from the point, and the number of edge intersections determines interior membership (odd count $\Rightarrow$ inside). A vehicle is assigned to the approach whose ROI contains its bounding-box centroid. Exclusion zones (e.g., medians, sidewalks) are defined as additional polygons; vehicles whose centroids fall within exclusion zones are removed from all metric computations.

3.11.2. Entry/Exit Event Detection

Crossing events are detected using the boundary-line sign-change method. For each approach, a counting line is defined by two endpoints $(\mathbf{p}_1, \mathbf{p}_2)$ and a direction vector $\mathbf{d}_{\text{from}}$ indicating the "from" side. At each frame, the dot product between the vehicle-to-line-midpoint vector and $\mathbf{d}_{\text{from}}$ determines the vehicle's side:

$$\text{side}(t) = \text{sign}\big((\mathbf{c}(t) - \mathbf{m}) \cdot \mathbf{d}_{\text{from}}\big), \tag{7}$$

where $\mathbf{c}(t)$ is the vehicle centroid at frame t and $\mathbf{m}$ is the line midpoint. A crossing event is registered when $\text{side}(t-1) \cdot \text{side}(t) < 0$ (sign reversal), indicating that the vehicle has traversed the boundary. The entry frame f_{entry} is recorded at the first boundary crossing, and the exit frame f_{exit} at the subsequent crossing of the opposite boundary.

3.11.3. Crossing Time Computation

The crossing time for vehicle i traversing from entry line L_a to exit line L_b is computed as:

$$T_{\text{cross},i} = \frac{f_{\text{exit}} - f_{\text{entry}}}{\text{FPS}}, \tag{8}$$

where FPS is the video frame rate. The actual crossing time $T_{\text{actual},d}(t)$ used in EFR computation (Equation (2)) is the harmonic mean of individual crossing times within the aggregation interval:

$$T_{\text{actual},d}(t) = \frac{n}{\sum_{i=1}^{n} T_{\text{cross},i}^{-1}}, \tag{9}$$

where n is the number of completed crossings in the interval. In the case where $n = 0$ (no completed crossings), $T_{\text{actual},d}(t)$ is undefined. If operationally $M_d(t) > 0$ but $n = 0$, this indicates a blockage state where discharge is effectively zero, and thus $E_{v,d}(t)$ is assigned a value of 0.

3.11.4. Handling Fragmented Tracks and Re-Association

When a tracked vehicle is temporarily lost due to occlusion or detection failure, ByteTrack's Kalman filter maintains a predicted trajectory for up to 30 frames ($\approx$ 1 s at 30 FPS source rate). If the vehicle reappears within this persistence window and its predicted position matches the new detection (via IoU-based association), the original track ID is preserved and the crossing time computation continues seamlessly. Tracks that fragment beyond the persistence window are discarded from the crossing-time average to prevent inflated T_{actual} values. Additionally, a periodic ID cleanup removes stale track entries every 1500 frames to maintain computational efficiency. This conservative approach ensures that only complete, high-confidence trajectories contribute to the Velocity Efficiency Index.

4. Results

4.1. Dataset Summary

The empirical analysis draws on continuous video capture from a rooftop-mounted 4K camera overlooking the study intersection. Table 5 summarized the data collection parameters.

Table 5. Dataset summary and quality parameters.

Parameter	Value
Total observation period	25 days
Days discarded (power outage)	4 days
Usable observation days	21 days
Daily coverage	06:00–22:00 (16 h)
Total usable hours	≈336 h
Signal cycles analyzed	>6000 cycles
Total vehicle detections	>1.2 million
Temporal resolution	1-min aggregation

Data from four days were discarded due to power outages that caused incomplete daily records. The remaining 21 days provide sufficient statistical power for the temporal and directional analyses presented below.

4.2. The Divergence of Kinematics and Flow

To understand the relationship between volume and discharge quality, we analyzed the temporal evolution of flow rate $F_d(t)$ and Flow Ratio $R_d(t)$, as illustrated in Figure 4. A critical observation from this analysis is the frequent decoupling of these two variables. Specifically, during several green phases, the flow rate remains elevated which indicates high volume throughput, yet the Flow Ratio exhibits sharp, high-frequency oscillations.

This divergence signifies "hidden inefficiencies" within the traffic stream. While the high flow rate suggests productivity, the volatile Flow Ratio reveals that the queue is actually experiencing stop-and-go shockwaves rather than smooth discharge. This behavior arises from heterogeneous friction sources, including rickshaws changing lanes or pedestrians filtering through traffic. These impediments force the stream to pulse rather than flow continuously. Traditional volume counts often smooth over these pulses through temporal aggregation, presenting a false picture of operational stability. In contrast, the Flow Ratio metric successfully captures these micro-level dynamics that determine the true discharge quality.

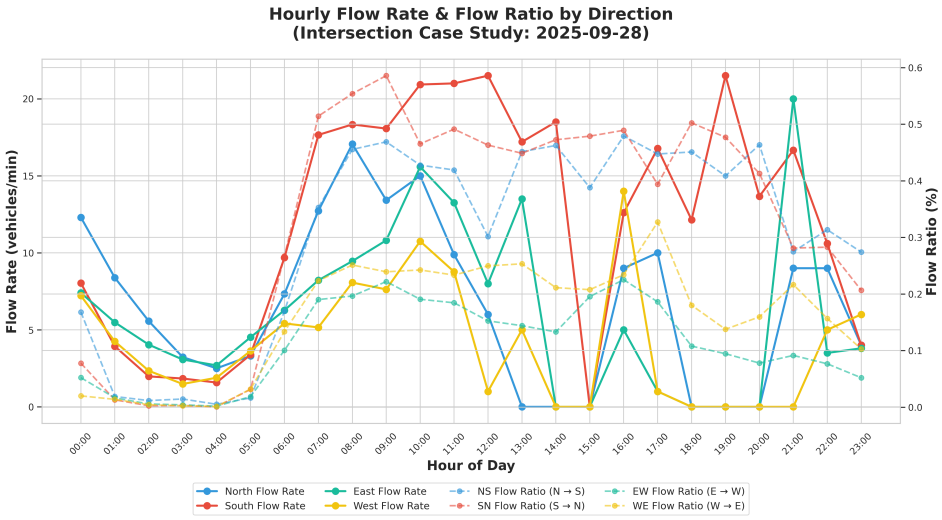

Figure 4. Representative temporal trends of flow rate and Flow Ratio. Divergence highlights hidden inefficiencies.

4.3. Temporal Instability and Correlation Collapse

To examine the temporal stability of the relationship between flow rate and Effective Flow Ratio, we computed rolling Pearson correlation using a 30-min sliding window, as presented in Figure 5. The analysis reveals substantial temporal instability in the flow-EFR relationship. Rather than hovering around a stable positive value, the correlation coefficient frequently plunges below the 0.3 threshold (marked in red) and occasionally enters negative territory.

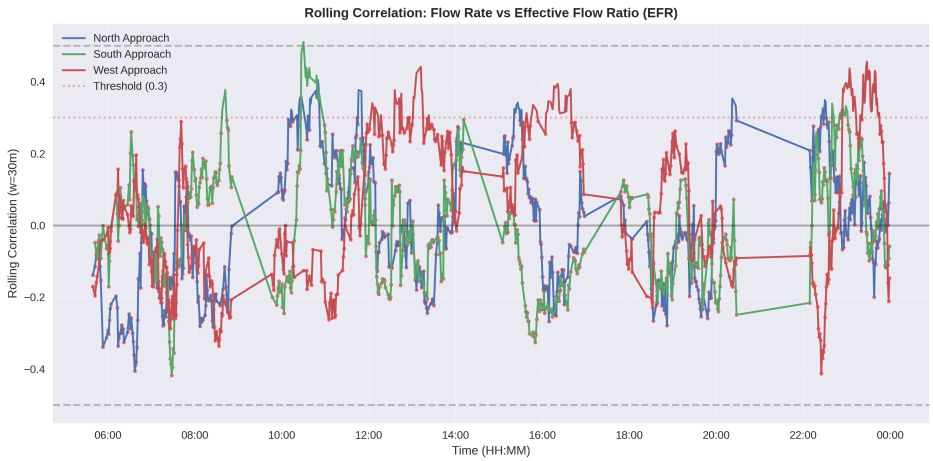

Figure 5. Rolling correlation between flow rate and Effective Flow Ratio (EFR) with 30-min window. Red markers indicate intervals where correlation drops below 0.3 threshold, signaling temporal instability in the flow–efficiency relationship.

Across the full dataset, the mean correlation coefficient was $\bar{\rho} = 0.24$ (95% CI: $[0.19, 0.29]$, $p < 0.001$), confirming a weak but statistically significant positive relationship. However, the high variance ($\sigma_\rho = 0.31$) and frequent excursions into negative territory underscore the temporal instability of this relationship.

These negative correlation intervals are particularly diagnostic, representing a regime where increasing flow rate leads to a decrease in EFR—the definition of hyper-congestion or flow breakdown. These periods correspond to "mixed-traffic friction," where the sheer density of agents causes an interlocking effect that stifles movement efficiency despite high demand. This phenomenon mirrors jamming in granular flows: beyond a critical density,

lateral interference dominates, and additional vehicles reduce rather than increase effective discharge. Consequently, this instability confirms that static capacity models are inadequate for mixed traffic, as the system transitions between efficiency regimes too rapidly for fixed parameters to capture.

4.4. The Non-Monotonic Efficiency Frontier

To directly test whether higher demand translates into higher efficiency, we binned flow rate observations and examined EFR distributions within each bin, as presented in Figure 6. The most significant finding from this analysis is the revelation of a non-monotonic relationship, which contradicts the standard assumption that higher utilization yields higher efficiency up to capacity. Instead, we observe a complex, regime-dependent pattern.

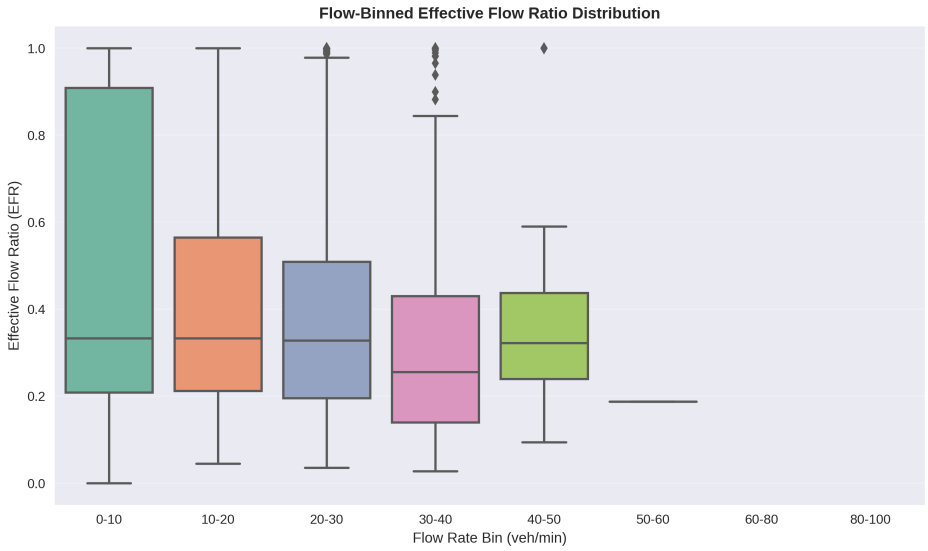

Figure 6. Flow-binned distribution of Effective Flow Ratio (EFR). Box plots show EFR variance within discrete flow-rate ranges. The non-monotonic pattern demonstrates that higher flow does not guarantee higher efficiency.

The underlying dynamics driving these distinct operational states are detailed below:

- **Low Flow (0–10 veh/min):** Variance is extreme. EFR spans the full range $[0, 1]$, reflecting the stochastic nature of low-demand arrival patterns and sporadic signal-pedestrian conflicts.
- **Moderate Flow (10–40 veh/min)—The "Zone of Chaos":** EFR variance remains high, but the median suppresses. This is the most operationally complex regime. At moderate densities, the heterogeneous interactions (e.g., speed differentials between cars traveling at 40 km/h and rickshaws at 15 km/h) maximize lateral interference, preventing the formation of stable platoons. Vehicles cannot accelerate to free-flow speed due to frequent encroachment by slower agents, yet density is insufficient to enforce orderly queuing. This is the regime where *heterogeneity penalty is maximized*.
- **High Flow (>40 veh/min)—The "Efficiency Ceiling":** Variance collapses, but crucially, the median EFR remains low (<0.4). This confirms an efficiency ceiling inherent to mixed traffic. Even at maximum throughput, the mixed-traffic stream cannot achieve the discharge quality of a homogeneous stream. The system hits a *friction limit before it hits a volume limit*. High flow is sustained not through velocity but through density—vehicles pack tightly and creep through the intersection as a slow-moving mass.

This empirically confirms the core claim: higher flow does not guarantee higher movement efficiency in heterogeneous traffic, validating EFR as an essential complement

to volume-based metrics. This finding directly contradicts the implicit assumption in capacity-based models that higher flow implies higher operational quality.

4.5. Visualizing the "Efficiency Paradox"

To visualize the non-linear relationship between demand, efficiency, and latency, we constructed a multi-dimensional efficiency surface as presented in Figure 7. This visualization exposes the "Efficiency Paradox," where a distinct operational region exists characterized by the coexistence of high flow rates, high latency, and low Flow Ratio. This specific zone corresponds to "productive congestion," a state where the intersection pushes high vehicle volumes but at a severe cost to user delay.

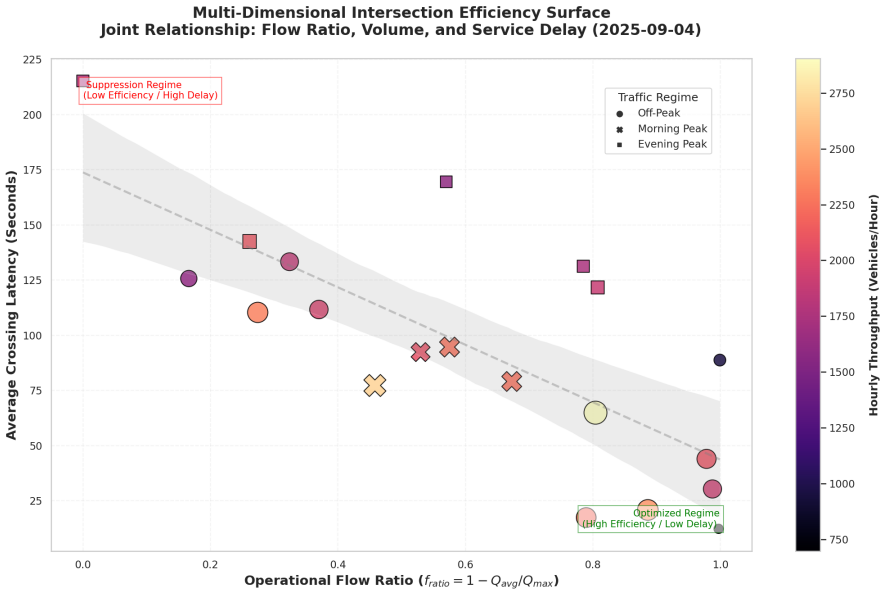

Figure 7. Multi-Dimensional Efficiency Surface showing the relationship between Flow Rate, Flow Ratio, and Average Crossing Time. The surface curvature highlights the "Efficiency Paradox" where high flow can coexist with high latency (low efficiency). This visualization serves to identify operational 'sweet spots' where efficiency is maximized, rather than acting as a quantitative prediction tool.

In homogeneous traffic models, high flow typically implies optimal speed, which aligns with the capacity state on the fundamental diagram. However, in mixed traffic, high flow is often achieved via a dense, slow-moving wall of vehicles that maintain minimal headways while crawling at sub-optimal velocities. EFR successfully distinguishes this high-latency state from true efficient discharge, a critical distinction that standard volume metrics miss entirely. Therefore, the surface serves primarily for the conceptual visualization of regime separation rather than precise quantitative inference. The practical utility lies in revealing that intermediate flow rates can achieve higher EFR than maximum flow rates when motion quality is preserved.

4.6. Operational Regimes and Discorrelation

The operational breakdown of the intersection through the lens of EFR is shown in Figure 8. Unlike flow rate alone, this efficiency-based segmentation separates smooth discharge from hidden inefficiency, revealing complex behaviors that standard volume counts fail to capture.

The scatter plot reveals three distinct operational regimes that flow rate alone cannot distinguish:

- **Smooth Discharge (Green):** High flow associated with high EFR (>0.7), indicating optimal green time utilization.

- **Hidden Inefficiency (Red):** High flow rate coexisting with low EFR (<0.4). In these cases, volume counts suggest productivity, but vehicles are essentially creeping or stalled by friction, failing to clear the intersection effectively.
- **Suppressed Demand (Blue):** Low flow and low EFR, typical of signal red phases or starved approaches.

The overall negative correlation ($r = -0.087$, 95% CI: $[-0.11, -0.06]$, $p < 0.001$) is statistically significant and suggests that efficiency exhibits weak linear association with demand in mixed traffic, rather than the positive correlation implicitly assumed by volume-based metrics. Although the magnitude of r is small, its statistical significance combined with regime clustering indicates regime-dependent, non-linear behaviour rather than a simple linear relationship. While the effect size is small, the direction contradicts the implicit assumption that higher throughput implies better performance. We note that time-series autocorrelation in minute-level aggregated data may inflate the apparent significance of Pearson r; the reported values characterize observed marginal patterns and should not be interpreted as evidence of statistical independence between flow and efficiency.

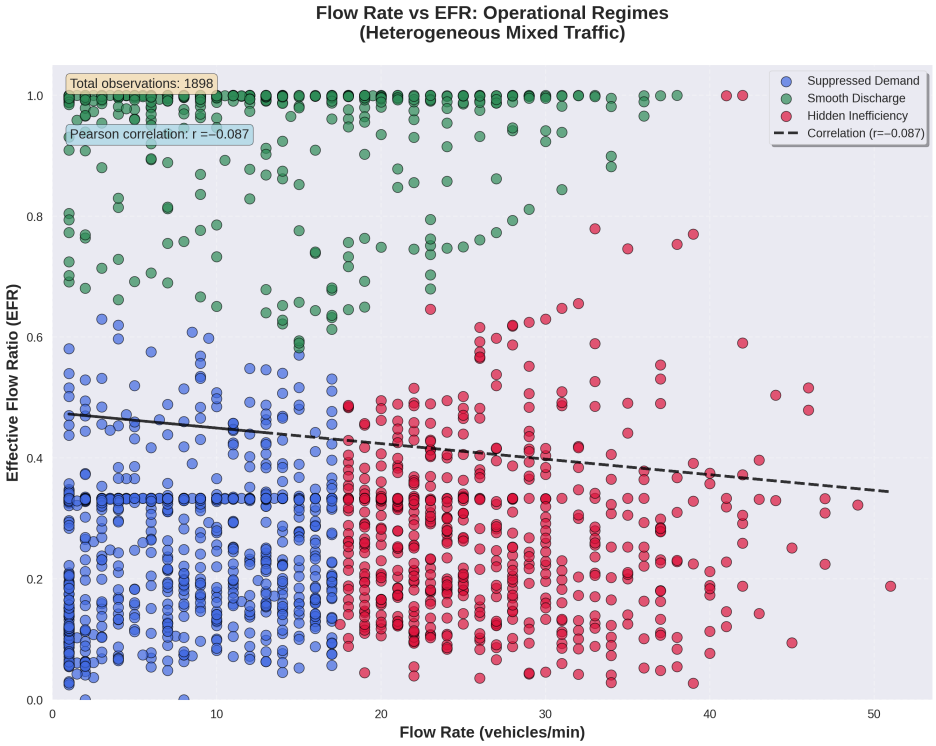

Figure 8. Flow Rate vs. EFR scatter plot showing three distinct operational regimes. Unlike flow rate alone, EFR separates smooth discharge from hidden inefficiency.

4.7. Directional Discorrelation Analysis

A comprehensive analysis of the West approach reveals how flow–efficiency discorrelation manifests over time, as visualized in Figure 9. To spatially and temporally localize operational failures, we examined the specific divergence patterns in this approach. High-divergence periods, highlighted as red shaded areas in the top panel, correspond to intervals where flow rate remains stable or high while EFR collapses. This decoupling is significant and is quantified by a peak discorrelation strength of 0.964, confirming that volume alone is a poor proxy for performance during these critical windows.

Figure 9. Comprehensive discorrelation analysis for the West approach. (**Top**): Time series overlay of Flow Rate and EFR. (**Middle**): Scatter plot colored by hour. (**Bottom**): Divergence strength.

The temporal distribution of these events is not random. The middle scatter plot reveals distinct clusters by time of day, suggesting that friction on the West approach is driven by recurrent impediments, such as scheduled bus arrivals or peak-hour pedestrian surges, rather than random noise. This recurring pattern implies that the current static signal plan systematically misallocates green time during these specific windows. Unlike delay or LOS metrics which struggle with queue boundary estimation, EFR proves robust under the heavy occlusion and non-lane-based traffic conditions common to this approach.

5. Discussion

5.1. The Decoupling of Flow and Efficiency

The central theoretical insight of this study is the dynamic decoupling of flow rate and discharge efficiency. In lane-based, homogeneous traffic, flow and speed are coupled via the fundamental diagram—as density increases towards critical density, flow increases and speed decreases predictably. Our data suggest that in mixed traffic, this coupling is fractured by lateral friction. The "Efficiency Paradox" observed in Figure 7 demonstrates that high volume can be sustained even as discharge quality (EFR) collapses. This implies that "Capacity" in mixed traffic is not a fixed number but a probabilistic state dependent on the instantaneous composition of the stream (e.g., the ratio of rickshaws to buses). EFR serves as a real-time probe of this state, offering a fidelity that static saturation flow estimates cannot match.

5.2. Implications for Adaptive Signal Control

Current Adaptive Traffic Signal Control (ATSC) systems, such as SCOOT or SCATS, typically optimize for Degree of Saturation (v/c) or queue length. Applying these logic structures to the Dhaka context is problematic because they assume that clearing the queue is equivalent to maximizing efficiency. However, as demonstrated by the divergence of flow and EFR earlier, green time is frequently wasted on phases that are locked by friction.

An EFR-based control logic would fundamentally alter the optimization objective. Conceptually, an EFR-informed control logic could be envisioned as follows: Instead of "Extend Green if Queue > 0," the logic would shift to "Extend Green if EFR $>$ Threshold."

It is important to reiterate that this control logic is not validated here but rather presented as a conceptual implication. If EFR drops despite the presence of a queue (indicating friction or blockage), it suggests the phase has become unproductive, preventing the accumulation of unproductive delay. This shift from volume-responsive to efficiency-responsive control is the key to potentially managing congestion in environments where infrastructure expansion is impossible. This does not imply premature termination during red-induced suppression but rather during green phases where motion efficiency collapses despite demand.

5.3. Practical Applications and Transport Planning

Beyond theoretical contributions, the EFR metric offers immediate practical value for transport agencies operating in mixed-traffic environments:

- **Cycle-Level Performance Auditing:** EFR enables per-cycle evaluation of signal efficiency, identifying specific phases where allocated green time fails to produce effective discharge. This granularity supports evidence-based signal retiming without requiring expensive simulation studies.
- **Bottleneck Identification:** The directional discorrelation analysis (Section 4.7) demonstrates how EFR can pinpoint approaches with recurrent friction problems, guiding targeted interventions such as pedestrian management or NMT lane separation.
- **Before-After Evaluation:** Unlike traditional counts that may show unchanged volumes, EFR can quantify whether infrastructure or policy interventions (e.g., rickshaw-free zones, pedestrian signal phases) genuinely improve discharge quality.
- **Real-Time Dashboard Integration:** The minute-level temporal resolution makes EFR suitable for integration into traffic management center dashboards, providing operators with actionable efficiency indicators alongside conventional volume displays.

5.4. EFR vs. Highway Capacity Manual LOS Framework

The Highway Capacity Manual's density-based Level of Service (LOS) metrics presume lane discipline and homogeneous vehicle behavior. In the observed data, traditional LOS classification would categorize many high-flow periods as LOS C or D (acceptable service), yet EFR reveals these same periods as operationally inefficient (EFR < 0.4). This demonstrates that EFR successfully maps operational states that LOS cannot distinguish, providing finer granularity for heterogeneous traffic diagnosis. Unlike LOS, which relies on calibrated speed-density relationships, EFR is derived directly from observed motion dynamics, making it robust to the compositional variance of mixed traffic.

5.5. Scalability, Limitations, and Platform Considerations

While EFR offers significant diagnostic power, its reliance on computer vision introduces specific constraints that inform deployment decisions.

5.5.1. Platform Selection: Rooftop vs. Ground-Level Cameras

The study employed a fixed rooftop-mounted camera at 55 m altitude rather than ground-level pole cameras. This choice was driven by the fundamental limitations of ground-level sensing in mixed traffic:

- **Severe Occlusion:** Ground cameras placed at typical 5–8 m pole heights suffer extensive occlusion from buses, trucks, and overlapping vehicles. In our preliminary ground-camera tests, occlusion losses exceeded 40% of vehicles during peak periods, rendering Flow Ratio computation unreliable.
- **Re-identification Challenges:** Ground-level multi-camera systems require robust vehicle re-identification across camera views to track crossing times. In heterogeneous

traffic with many similar-appearing vehicles (e.g., identical rickshaw models), re-ID accuracy degrades substantially, introducing systematic errors in T_{actual} estimation.

- **Infrastructure Cost:** Achieving comparable coverage to a single elevated camera would require 4–6 coordinated ground cameras with complex calibration and synchronization, substantially increasing deployment cost and maintenance burden.

The rooftop installation provides near-orthogonal BEV imagery that eliminates these constraints. While not universally available, suitable vantage points exist in many urban contexts (adjacent buildings, elevated walkways, existing CCTV structures). The methodology remains camera-agnostic: any platform providing BEV transformation capability can implement EFR computation.

5.5.2. Tracker Dependence and Failure Modes

The accuracy of EFR is contingent on the stability of the ByteTrack multi-object tracker. While the 55m aerial perspective mitigates the severe occlusion issues typical of ground-level sensing (where tall vehicles block entire lanes), challenges persist in scenarios of "hyper-dense clustering." In these high-density states, tight clusters of smaller vehicles (e.g., motorcycles and rickshaws) moving synchronously alongside large buses may visually merge or fall below the minimum inter-object separation threshold of the detector. This semantic overlap, rather than simple geometric occlusion, represents the primary tracking failure mode in aerial BEV imagery, potentially leading to an underestimation of N_d. The 98% tracking success rate reported in Section 3.10 mitigates this concern significantly, but future work will incorporate uncertainty quantification to flag low-confidence EFR estimates in these specific regimes.

5.5.3. Parameter Calibration

The T_{ideal} parameter requires calibration based on intersection geometry. While we have demonstrated a geometry-based derivation ($T_{\text{ideal}} = L/v_{\text{free}}$), future work will focus on automating this calibration using self-supervised learning to establish baseline free-flow velocities for any given camera deployment.

5.5.4. Ethical Considerations and Privacy

The 55 m elevation provides a critical privacy advantage: at this altitude, individual faces are not identifiable in the captured imagery (<10 pixels per face), and license plates are unreadable. The system processes aggregate motion patterns rather than individual identification. No biometric data is collected, stored, or processed. The research protocol was designed to collect only traffic flow statistics, not personally identifiable information, aligning with privacy-by-design principles for urban sensing applications.

6. Conclusions

This study addressed the critical limitation of traditional traffic performance metrics in heterogeneous, mixed-traffic environments: their inability to distinguish between effective vehicular discharge and varying states of congestion. By leveraging a computer-vision framework combining YOLOv11 and ByteTrack deployed on a fixed rooftop camera, we introduced and validated two novel state variables: **Flow Ratio**, a measure of kinematic presence, and **Effective Flow Ratio (EFR)**, a measure of operational discharge quality.

Our empirical analysis of a major intersection in Dhaka, Bangladesh, yielded two definitive conclusions:

1. **Flow rate and efficiency are dynamically decoupled in mixed traffic.** High demand does not guarantee high discharge quality. The "Efficiency Paradox" demonstrates

that high volume can coexist with severe user delay when vehicles move as a dense, slow-moving mass rather than a smooth stream.

2. **This decoupling is non-monotonic and temporally unstable.** The flow–efficiency relationship exhibits rapid regime shifts characterized by negative correlation intervals (hyper-congestion) and high-variance moderate-flow regimes ("zone of chaos"). Static signal plans cannot accommodate this instability.

We conclude that efficiency in heterogeneous traffic is an emergent property of motion quality, not a direct derivative of volume. As cities in the developing world seek to modernize their transportation infrastructure, the integration of EFR-based monitoring represents a low-cost, high-impact strategy to unlock latent capacity without major infrastructure investment. This work provides the foundational metrics required to transition Intelligent Transportation Systems (ITS) from volume-based logic to efficiency-based logic, paving the way for next-generation adaptive signal control in the complex traffic landscapes of the Global South.

Future work will focus on: (i) integrating EFR into real-time adaptive control policies that optimize for movement efficiency rather than volume alone; (ii) extending validation across multiple intersections and network scales to establish generalizability; (iii) developing composite performance indices that combine EFR with safety and environmental metrics for comprehensive intersection assessment; and (iv) automating parameter calibration through self-supervised learning to reduce deployment effort.

Author Contributions: Conceptualization, A.A.I.S. and T.A.; methodology, A.A.I.S. and T.A.; software, A.A.I.S.; validation, A.A.I.S., T.A. and M.N.H.; formal analysis, A.A.I.S.; investigation, T.A.; resources, A.A.I.S. and T.A.; data curation, A.A.I.S. and T.A.; writing—original draft preparation, A.A.I.S. and T.A.; writing—review and editing, A.A.I.S., T.A. and M.N.H.; visualization, A.A.I.S. and T.A.; supervision, T.A. and M.N.H.; project administration, A.A.I.S.; funding acquisition, A.A.I.S. and M.N.H. All authors have read and agreed to the published version of the manuscript.

Funding: This research received no external funding.

Institutional Review Board Statement: Ethical review and approval were waived for this study as it involved the observation of public traffic infrastructure without interaction with human subjects. The data collection was authorized under specific operational permits granted by the Dhaka North City Corporation and the Dhaka Metropolitan Police.

Informed Consent Statement: Individual subject consent was waived due to the observational nature of the study. The data collection protocol adhered to privacy-by-design principles: the rooftop camera installation height (55 m) resulted in a Ground Sampling Distance (GSD) insufficient to resolve Personally Identifiable Information (PII), such as facial features or vehicle license plates.

Data Availability Statement: Restrictions apply to the availability of the raw video data generated during this study to ensure compliance with local data privacy regulations. Anonymized derived data (e.g., vehicle trajectory logs, ROI masks, and computed EFR metrics) are available from the authors upon reasonable request.

Acknowledgments: The authors acknowledge the support of Dhaka North City Corporation and Dhaka Metropolitan Police for granting permission to conduct the field study at Gulshan 1 intersection. We also thank TraffiX for maintaining the deployed signal control and sensing systems and Sigmind for providing technical assistance in data collection and computer vision model integration.

Conflicts of Interest: Authors Abu Anas Ibn Samad and Tanvir Ahmed are employed by SIGMIND. The remaining author declares no commercial or financial relationships that could be construed as a potential conflict of interest.

Abbreviations

The following abbreviations are used in this manuscript:

LOS	Level of Service
BEV	Bird's-Eye View
EPP	Exclusive Pedestrian Phasing
CPP	Concurrent Pedestrian Phasing
HCM	Highway Capacity Manual
DoS	Degree of Saturation
YOLO	You Only Look Once
SORT	Simple Online and Realtime Tracking
MOT	Multi-Object Tracking
ATSC	Adaptive Traffic Signal Control
ITS	Intelligent Transportation Systems
NMT	Non-Motorized Traffic
EFR	Effective Flow Ratio

Appendix A. ROI Configuration

To ensure reproducibility of the spatial filtering and counting logic, we provide the exact vertex coordinates used in the deployed system. All coordinates are in the 960×960 pixel image domain.

Appendix A.1. Counting Lines

Table A1 lists the start and end coordinates for the directional counting lines used to detect vehicle entry and exit events.

Table A1. Counting Line Coordinates (Image Domain).

Line ID	Start Point (x, y)	End Point (x, y)	Direction Vector
W	(445.2, 704.0)	(562.8, 524.8)	$(-0.65, -0.76)$
S	(570.0, 499.2)	(445.2, 328.5)	$(-0.61, 0.79)$
E	(423.6, 328.5)	(316.8, 469.3)	$(0.60, 0.80)$
N	(307.2, 490.7)	(428.4, 710.4)	$(0.71, -0.70)$
WN	(430.8, 945.1)	(435.6, 808.5)	$(-1.00, -0.06)$
WS	(620.4, 571.7)	(674.4, 580.3)	$(-0.09, 1.00)$
ES	(433.2, 285.9)	(435.6, 226.1)	$(1.00, 0.07)$
NE	(230.4, 520.5)	(277.2, 531.2)	$(0.13, -0.99)$

Appendix A.2. Region of Interest (ROI) Polygons

Table A2 provides the vertex definitions for the approach regions (NS, WE, SN, EW) and exclusion zones (X1, X2, X3).

Table A2. ROI Polygon Vertices.

Region ID	Vertex Coordinates $\{(x_1, y_1), \ldots, (x_n, y_n)\}$
NS (North Approach)	{(8.4, 789.3), (212.4, 650.7), (292.8, 546.1), (345.6, 631.5), (202.8, 817.1), (32.4, 919.5)}
WE (West Approach)	{(490.8, 746.7), (552.0, 646.4), (648.0, 814.9), (693.6, 940.8), (598.8, 951.5)}
SN (South Approach)	{(518.4, 388.3), (636.0, 247.5), (760.8, 196.3), (778.8, 262.4), (690.0, 320.0), (570.0, 482.1)}
EW (East Approach)	{(344.4, 384.0), (295.2, 283.7), (278.4, 232.5), (337.2, 196.3), (403.2, 300.8)}
X1 (Exclusion)	{(789.6, 951.5), (956.4, 953.6), (950.4, 224.0), (758.4, 317.9), (710.4, 360.5), (679.2, 501.3)}
X2 (Exclusion)	{(272.4, 2.1), (914.4, 4.3), (888.0, 96.0), (454.8, 228.3), (336.0, 172.8)}
X3 (Exclusion)	{(10.8, 770.1), (200.4, 648.5), (253.2, 486.4), (247.2, 266.7), (214.8, 128.0), (205.2, 6.4), (10.8, 12.8), (9.6, 761.6)}

References

1. Saha, A. Delay in Oversaturated Flow Condition at Signal Controlled Intersection under Heterogeneous Traffic Scenario. *Trasp. Eur.* **2022**, *87*, 15. [CrossRef]
2. Hossain, M. Estimation of saturation flow at signalised intersections of developing cities: A micro-simulation modelling approach. *Transp. Res. Part A Policy Pract.* **2001**, *35*, 123–141. [CrossRef]
3. Li, J.; Yu, C.; Shen, Z.; Su, Z.; Ma, W. A survey on urban traffic control under mixed traffic environment with connected automated vehicles. *Transp. Res. Part C Emerg. Technol.* **2023**, *154*, 104258. [CrossRef]
4. Leong, L.V.; Wan Ibrahim, W.H.; Mohd, A.F. Effect Of Motorcycles Travel Behaviour On Saturation Flow Rates At Signalized Intersections In Malaysia. In Proceedings of the 23rd ARRB Conference, Adelaide, Australia, 30 July–1 August 2008. Available online: https://trid.trb.org/view/885981 (accessed on 12 January 2026).
5. Singh, M.K.; Ramachandra Rao, K. Simulation of signalized intersection with non-lane-based heterogeneous traffic conditions using cellular automata. *Transp. Res. Rec.* **2024**, *2678*, 909–930. [CrossRef]
6. Agarwal, A.; Sahu, D.; Mohata, R.; Jeengar, K.; Nautiyal, A.; Saxena, D.K. Dynamic traffic signal control for heterogeneous traffic conditions using max pressure and reinforcement learning. *Expert Syst. Appl.* **2024**, *254*, 124416. [CrossRef]
7. Preethi, P.; Varghese, A.; Ashalatha, R. Modelling delay at signalized intersections under heterogeneous traffic conditions. *Transp. Res. Procedia* **2016**, *17*, 529–538. [CrossRef]
8. Zhai, C.; Wu, W.; Xiao, Y.; Zhang, J.; Zhai, M.; Wu, Y. A novel throttle-based self-stabilizing control scheme integrated into an anisotropic continuum model to mitigate cyber-attacks in connected vehicle scenarios. *Chaos Solitons Fractals* **2025**, *201*, 117319. [CrossRef]
9. Zhai, C.; Wu, W. Designing continuous delay feedback control for lattice hydrodynamic model under cyber-attacks and connected vehicle environment. *Commun. Nonlinear Sci. Numer. Simul.* **2021**, *95*, 105667. [CrossRef]
10. Ahsan, H.M.; Dey, A.C. Effects of Non-Motorized Vehicles (NMV) on a selected Intersection in Dhaka City for Non lane based heterogeneous traffic using (VISSIM 5.3). In Proceedings of the 4th International Conference on Advances in Civil Engineering (ICACE 2018), Chittagong, Bangladesh, 19–21 December 2018.
11. Rafa, M. The Influence of the Movement of Cycle-Rickshaws on Traffic Congestion. A Study of Heterogeneous Traffic Conditions in Mega-city Dhaka, Bangladesh. Master's Thesis, Erasmus University Rotterdam, Rotterdam, The Netherlands, 2020. Available online: http://hdl.handle.net/2105/56579 (accessed on 12 January 2026).
12. Okech, T.C. Modeled performance characteristics of heterogeneous traffic streams containing non-motorized vehicles. In Proceedings of the 82nd Annual Meeting of the Transportation Research Board, Washington, DC, USA, 12–16 January 2003.
13. Khan, S.I.; Maini, P. Modeling heterogeneous traffic flow. *Transp. Res. Rec.* **1999**, *1678*, 234–241. [CrossRef]
14. Rouphail, N.M.; Akcelik, R. More Signal Capacity With Less Green? *ITE J.* **1996**, *66*, 34–40.
15. Li, H.; Prevedouros, P.D. Detailed Observations of Saturation Headways and Start-Up Lost Times. *Transp. Res. Rec.* **2002**, *1802*, 44–53. [CrossRef]
16. Bhattacharyya, K.; Paul, B.; Maitra, B. Dynamics of Vehicle Discharge at Signalized Intersections with Nonlane-based Mixed Traffic Operations. *Asian Transp. Stud.* **2018**, *5*, 310–325. [CrossRef]
17. Hadiuzzaman, M.; Rahman, M.M.; Karim, M.A. Saturation flow model at signalized intersection for non-lane based traffic. *Can. J. Transp.* **2008**, *2*. Available online: https://journalhosting.ucalgary.ca/index.php/cjt/article/view/15851 (accessed on 12 January 2026).
18. Lin, F.-B.; Tseng, P.-Y.; Su, C.-W. Variations in queue discharge patterns and their implications in analysis of signalized intersections. *Transp. Res. Rec.* **2004**, *1883*, 192–197. [CrossRef]
19. Khanam, R.; Hussain, M. Yolov11: An overview of the key architectural enhancements. *arXiv* **2024**, arXiv:2410.17725. [CrossRef]
20. Zhang, Y.; Sun, P.; Jiang, Y.; Yu, D.; Weng, F.; Yuan, Z.; Luo, P.; Liu, W.; Wang, X. ByteTrack: Multi-object Tracking by Associating Every Detection Box. In *Computer Vision—ECCV 2022*; Avidan, S., Brostow, G., Cissé, M., Farinella, G.M., Hassner, T., Eds.; Lecture Notes in Computer Science; Springer: Cham, Switzerland, 2022; Volume 13682, pp. 1–21. [CrossRef]
21. Transportation Research Board. *Highway Capacity Manual 7th Edition: A Guide for Multimodal Mobility Analysis*; The National Academies Press: Washington, DC, USA, 2022. [CrossRef]
22. Lulusi, L.; Sugiarto, S.; Saleh, S.M.; Isya, M.; Rusdi, M.; Rahma, R. Bayesian MCMC with Gibbs sampling for saturation flow rate estimation in heterogeneous traffic at pretimed signalized intersections. *MethodsX* **2025**, *14*, 103507. [CrossRef]
23. Paul, S.; Kumar, V.; Chandrashekar, R.; Nagpal, A.; Khan, I.; Raed, R.; Sharma, N. Capacity of heterogeneous traffic in urban areas: A level of service estimation. *E3S Web Conf.* **2024**, *529*, 03012. [CrossRef]
24. Arun, A.; Madhu, E.; Velmurugan, S. Selection of a suitable service measure and determination of LOS criteria for Indian multilane interurban highways: A methodological review. *Transp. Dev. Econ.* **2016**, *2*, 16. [CrossRef]

25. Boora, A.; Ghosh, I.; Chandra, S.; Rani, K. Measurement of free-flow conditions on multilane intercity highways under heterogeneous traffic conditions. *J. S. Afr. Inst. Civ. Eng.* **2018**, *60*, 2–9. [CrossRef]
26. Kodupuganti, S.R. Modeling Operational Performance of Urban Roads with Heterogeneous Traffic Conditions. Ph.D. Dissertation, University of North Carolina at Charlotte, Charlotte, NC, USA, 2021. [CrossRef]
27. Chen, S.; Piao, L.; Zang, X.; Luo, Q.; Li, J.; Yang, J.; Rong, J. Analyzing differences of highway lane-changing behavior using vehicle trajectory data. *Phys. A Stat. Mech. Appl.* **2023**, *624*, 128980. [CrossRef]
28. Mahmud, M.S. Comparing the Operational Efficiency of Signalized Intersections with Exclusive and Concurrent Pedestrian Phase Operations Considering Pedestrian Non-Compliance. Master's Thesis, University of Pittsburgh, Pittsburgh, PA, USA, 2018. Available online: https://d-scholarship.pitt.edu/33296 (accessed on 12 January 2026).
29. Gårder, P. Pedestrian safety at traffic signals: A study carried out with the help of a traffic conflicts technique. *Accid. Anal. Prev.* **1989**, *21*, 435–444. [CrossRef]
30. Mohanty, M.; Pattanaik, M.L.; Samal, S.R.; Shivam. Assessing the Impact of Three-Wheelers on Traffic Flow in India: A Case Study Using ANN. *Komunikácie* **2024**, *26*, A50–A65. [CrossRef]
31. Maladkar, D.; Sai, A.; Nayak, S.; Udasi, S.N.; Muttal, C. Traffic Flow Detection and Prediction Using YOLO11: A Threshold-Based Approach for Identifying Traffic Levels. In Proceedings of the 3rd International Conference on Futuristic Technology, Kawasaki City, Japan, 21–22 February 2025. [CrossRef]
32. Hung, G.; Rodriguez, I.F. A Comparative Study of YOLOv8 to YOLOv11 Performance in Underwater Vision Tasks. *arXiv* **2025**, arXiv:2509.12682. [CrossRef]
33. Akyon, F.C.; Altinuc, S.O.; Temizel, A. Slicing Aided Hyper Inference and Fine-Tuning for Small Object Detection. In Proceedings of the 2022 IEEE International Conference on Image Processing (ICIP), Bordeaux, France, 16–19 October 2022; pp. 966–970. [CrossRef]
34. Abouelyazid, M. Comparative Evaluation of SORT, DeepSORT, and ByteTrack for Multiple Object Tracking in Highway Videos. *IJSICS* **2023**, *8*, 42–52. Available online: https://vectoral.org/index.php/IJSICS/article/view/97 (accessed on 12 January 2026).
35. Zhu, P.; Wen, L.; Du, D.; Bian, X.; Ling, H.; Hu, Q.; Nie, Q.; Cheng, H.; Liu, C.; Liu, X. VisDrone-DET2018: The Vision Meets Drone Object Detection in Image Challenge Results. In *Computer Vision—ECCV 2018 Workshops*; Leal-Taixé, L., Roth, S., Eds.; Lecture Notes in Computer Science; Springer: Cham, Switzerland, 2019; Volume 11133, pp. 437–468. [CrossRef]
36. Ibn Samad, A.A.; Ahmed, T. A Multi-Line Aggregated Tracking Approach for Vehicle Counting in Congested Urban Traffic. In Proceedings of the 2023 26th International Conference on Computer and Information Technology (ICCIT), Cox's Bazar, Bangladesh, 13–15 December 2023; pp. 1–6. [CrossRef]
37. Ahmed, T.; Sharmin Mou, F.; Ibn Samad, A.A. A Deep Learning Based Bangladeshi Vehicle Classification Using Fine-Tuned Multi-class Vehicle Image Network (MVINet) Model. In Proceedings of the 2023 International Conference on Next-Generation Computing, IoT and Machine Learning (NCIM), Gazipur, Bangladesh, 16–17 June 2023; pp. 1–6. [CrossRef]